

Vibration attenuation in a nonlinear flexible structure via nonlinear switching circuits and energy harvesting implications

Journal of Intelligent Material Systems and Structures

2019, Vol. 30(7) 965–976

© The Author(s) 2019

Article reuse guidelines:

sagepub.com/journals-permissions

DOI: 10.1177/1045389X19828835

journals.sagepub.com/home/jim



Tarcisio Silva¹, David Tan², Carlos De Marqui¹  and Alper Erturk² 

Abstract

We study the suppression of strongly nonlinear vibrations of a flexible structure by using nonlinear switching circuit techniques, namely the synchronized switch damping on short circuit and the synchronized switch damping on inductor circuit, as well as energy harvesting implications through the synchronized switch harvesting on inductor circuit combined with the same nonlinear structure. Nonlinear switching shunts have been mostly explored for suppressing linear resonance in flexible structures. However, such flexible structures can easily undergo undesired resonant bifurcations and exhibit co-existing large- and small-amplitude branches in their frequency response. In this work, we investigate a strongly nonlinear and weakly coupled flexible structure for suppressing its large-amplitude periodic response branch under primary resonance excitation. The synchronized switch damping on short circuit and synchronized switch damping on inductor circuit damping techniques are employed and compared with the baseline (near short circuit) frequency response. It is shown that the synchronized switch damping on inductor circuit can substantially reduce the large-amplitude branch, offering the possibility of entirely suppressing undesired bifurcations. Energy harvesting implications are also explored by using the same structure as a wideband energy harvester. While the harvested power can be boosted with a synchronized switch harvesting on inductor circuit, the large-amplitude branch of the harvester is significantly shortened due to the strong shunt damping effect as a trade-off.

Keywords

Vibration, piezoelectricity, damping, energy harvesting, nonlinear

1. Introduction

The dissipation of undesired structural vibrations is of interest in a variety of engineering applications ranging from industrial machines to aerospace structures. Especially for lightweight flexible structures used in aircraft and spacecraft systems, piezoelectric shunt damping (Ahmadian and Deguilio, 2001; Lesieutre, 1998) offers remarkable advantages as an electronic damping approach without mass loading effects of conventional and bulky vibration damping methods (Jones, 2001; Nashif et al., 1985). Especially after the 1990s, piezoelectric shunt damping was studied for structures ranging from experimental beam setups (Hagood and von Flotow, 1991) to aircraft panels (Wu et al., 2000) and space truss structures (Hagood and Crawley, 1991), yielding several successful results. Various types and applications of piezoelectric shunt damping can be found in review articles by Lesieutre (1998) and Ahmadian and Deguilio (2001).

Piezoelectric shunt damping is applied by connecting a passive (or semi-passive) electrical circuit to the electrode terminals of a piezoelectric interface (e.g. patch or stack) that is attached to the main (host) structure (Ahmadian and Deguilio, 2001; Lesieutre, 1998). Electrically, a piezoelectric element itself is a capacitive element in static conditions, and therefore, its capacitive behavior inherently couples with the respective shunt circuit. For instance, using a resistor alters the stiffness and damping of the structure and dissipates energy

¹Department of Aeronautical Engineering, São Carlos School of Engineering, University of São Paulo, São Carlos, Brazil

²The George W. Woodruff School of Mechanical Engineering, Georgia Institute of Technology, Atlanta, GA, USA

Corresponding author:

Alper Erturk, The George W. Woodruff School of Mechanical Engineering, Georgia Institute of Technology, Atlanta, GA 30332, USA.
Email: alper.erturk@me.gatech.edu

through Joule heating. The resistive shunting concept was first used by Uchino and Ishii (1988), and its effect on the structure is analogous to constraint-layer-damping treatments. Capacitive shunting results in a variation of structural stiffness with changing external capacitance (Lesieutre, 1998). Changing structural stiffness alters the resonance frequencies of the structure but damping is not affected. Inductive shunting was first studied by Forward (1979), and it was shown that the inductance can be selected to cancel the internal piezoelectric capacitance, yielding an undamped dynamic vibration absorber effect. Knowing from Uchino and Ishii (1988) that a resistor could be used to create damping effect, Hagood and von Flotow (1991) connected a resistor and inductor in series to realize the damped dynamic vibration absorber effect (as an electromechanical analog of the well-known Den Hartog vibration absorber). Wu (1996) proposed connecting the resistor and inductor in parallel as an alternative resistive-inductive shunt circuit. The result was again a damped dynamic vibration absorber but the damping trend of shunt resistance (as compared to series) was reversed. The resistive-inductive shunt circuits (series/parallel) have received the most attention (Lesieutre, 1998), as they create the damped dynamic vibration absorber effect for proper selection of inductance and resistance. More recently, such inductive circuits have been employed in locally resonant piezoelectric metamaterials and metastructures (Sugino et al., 2017) for low-frequency band gap formation.

Following the aforementioned linear piezoelectric shunt damping circuits, synchronized switching damping (SSD) techniques (Guyomar et al., 2009; Lefeuve et al., 2006; Richard et al., 1999, 2000) and state-switched shunts (Clark, 2000; Corr and Clark, 2002; Cunefare et al., 2000) were developed in order to overcome the limitations and enhance the capabilities of entirely passive strategies (note that another body of work investigated nonlinear capacitance/inductance (Soltani and Kerschen, 2015; Lossouarn et al., 2017) and essentially nonlinear piezoelectric shunt circuitry (Zhou et al., 2014) for targeted energy transfer (Vakakis et al., 2008)). In particular, the SSD techniques introduced by Richard et al. (1999, 2000) exploit the nonlinear treatment of the electrical output of piezoelectric elements and result in an increase in the mechanical-to-electrical energy conversion in systems with weak electromechanical coupling. As a result, more recently, synchronized switching was successfully implemented by Guyomar et al. (2005) for energy harvesting performance enhancement as well. In most of these efforts, nonlinear switching circuits have so far been effectively used for damping of linear resonant structures and for energy harvesting enhancement in weakly coupled mechanically linear energy-harvester structures. Both shunt damping and energy harvesting performance of these circuits remain rather unexplored

in the existing literature for nonlinear structures although such flexible structures often exhibit strong nonlinearities, bifurcations, and multi-valued response in real-world applications. In this work, we explore the effectiveness of the semi-passive synchronized switch damping on short (SSDS) and the synchronized switch damping on inductor (SSDI) circuits for suppressing large-amplitude vibrations of a strongly nonlinear flexible structure. The focus is placed on the large-amplitude branch in the co-existing response region in the frequency domain. These circuits are studied for the possibility of suppressing nonlinear bifurcations of the structure both numerically and experimentally. Finally, energy harvesting implications are also explored using the synchronized switch harvesting on inductor (SSHI) circuit with the same flexible nonlinear structure as a wideband harvester.

2. Nonlinear flexible structure and experimental setup

The schematic and the picture of the nonlinear structure of interest are shown in Figures 1 and 2, and it was recently proposed and explored by Leadenham and Erturk (2015) for broadband vibration energy harvesting with a focus on its primary and secondary resonance behaviors through experiments as well as modeling and analysis using the method of harmonic balance. This flexible structure undergoes resonant bifurcations (Guckenheimer and Holmes, 2013; Nayfeh and Balachandran, 2008) and exhibits the jump phenomenon (in the form of overall hardening) even for very low base acceleration inputs (on the order of tens of milli-g) (Leadenham and Erturk, 2015; Silva et al., 2016). Here, the same structural platform is used for the application of SSDS/SSDI (Richard et al., 1999, 2000) circuits to suppress undesired large-amplitude vibrations and then for energy harvesting using the SSHI circuit (Guyomar et al., 2005). The three-dimensional (3D) model and the lumped-parameter representation of this structure are shown in Figure 1(a) and (b), respectively. Figure 2(a) shows the experimental structure mounted to the armature of a long-stroke shaker through its clamp. The nonlinear stiffness behavior of the bent beam that causes the large-amplitude vibrations is shown in Figure 2(b). It is worth mentioning that large-amplitude vibrations result in nonlinear dissipative effects (due to air drag as well (Bandstra, 1983)), as indicated in Figure 1(b).

This flexible structure is made from 25.4 mm wide by 0.254 mm thick AISI 1075 spring steel and is approximately 20-cm long. The steel is cut and bent using common sheet metal tools. The bend angles used are small enough to allow near zero radius bends without prior heating the metal. The lumped mass attachment consists of pieces of stainless steel, bolted

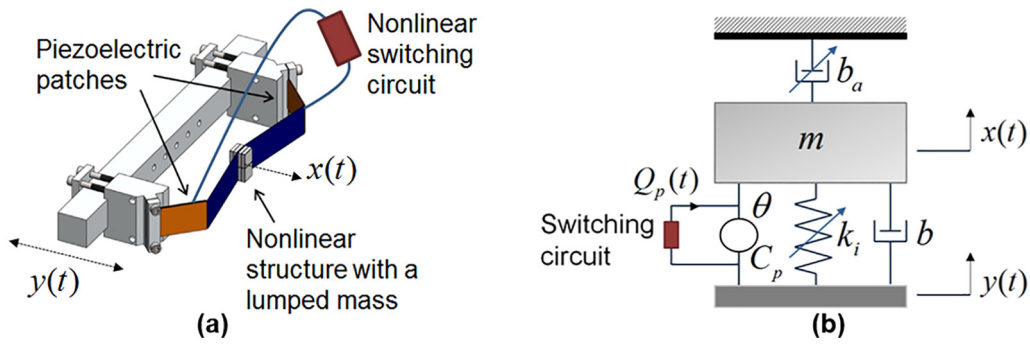


Figure 1. (a) 3D model of the nonlinear structure explored in this work with a nonlinear switching (SSDS/SSDI/SSHI) circuit and (b) lumped-parameter representation with nonlinear stiffness and air damping components.

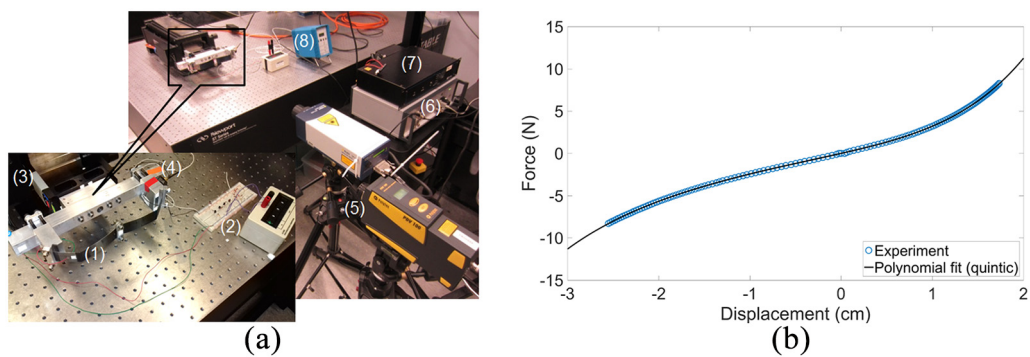


Figure 2. (a) Experimental setup: (1) weakly coupled nonlinear structure with piezoelectric patches; (2) nonlinear SSDS/SSDI/SSHI circuit; (3) vibration exciter (electrodynamics shaker); (4) accelerometer; (5) laser Doppler vibrometers; (6) vibration control unit (using base acceleration as the feedback signal); (7) power amplifier; (8) signal conditioner; and (b) experimentally measured strongly nonlinear stiffness behavior with a quintic polynomial fit.

together sandwiching the center of the beam. Both ends of the bent beam are clamped. Electromechanical coupling is due to four piezoelectric patches bonded near the clamps, resulting in two bimorphs (each one with two piezoelectric layers in series connection) that are weakly coupled to the structure. The bimorphs are then combined in parallel to each other and to the external circuit. The structure is shunted to the switching (SSDS/SSDI/SSHI) circuit through the piezoelectric interface. It is important to highlight that this structure is taken as a specific and convenient configuration to explore the effectiveness of the switching circuits without loss of generality for implementation to other flexible monostable Duffing-like (Kovacic and Brennan, 2011) nonlinear structures that exhibit strongly nonlinear behavior and the jump phenomenon.

The nonlinear structure is modeled as a single-degree-of-freedom system with linear viscous and quadratic damping terms, a nonlinear elastic restoring force (Figure 2(b)), and linear electromechanical coupling undergoing base excitation

$$m\ddot{z} + b\dot{z} + b_a|\dot{x}|\dot{x} + F_s(z) - \theta v = -m^*\ddot{y} \quad (1)$$

$$C_p\dot{v} + \dot{Q}_p + \theta z = 0 \quad (2)$$

where m is the equivalent mass of the device, m^* is the effective mass that causes the forcing term due to base excitation ($m = m^*$, if the lumped mass dominates the mass of the rest of the structure), b is the linear viscous damping coefficient, b_a is the quadratic damping coefficient, $y(t)$ is the base displacement measured in an inertial frame, $z(t)$ is the displacement of the oscillator relative to the moving base, v is the voltage across the resultant of the piezoelectric electrodes, and an overdot represents differentiation with respect to time. Furthermore, C_p is the equivalent piezoelectric capacitance, θ is the electromechanical coupling, $Q_p(t)$ is the electric charge, and $F_s(z)$ is the nonlinear elastic restoring force experimentally identified as the following equation (Leadenham and Erturk, 2015):

$$F_s(z) = k_1z + k_2z^2 + k_3z^3 + k_4z^4 + k_5z^5 \quad (3)$$

Note that the displacement of the mass relative to the fixed reference frame is denoted by $x(t)$ in Figure 1(b); therefore, the displacement relative to the base is $z(t) = x(t) - y(t)$. The predominant nonlinear stiffness

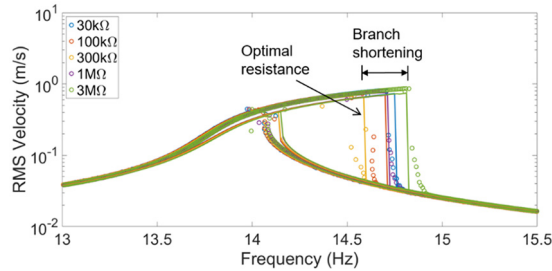


Figure 3. Effect of resistive shunt damping on large-amplitude nonlinear vibration response of the structure (in up-sweep). The damping effect of Joule heating from resistive shunting (typical scenario in energy harvesting (Leadenham and Erturk, 2015)) results in a very limited shortening of the large-amplitude nonlinear vibration branch.

behavior is cubic (as in a monostable Duffing oscillator) and the quadratic term in equation (3) results from the structural asymmetry, while the quartic and quintic terms are merely for further accuracy. Further details and linear/nonlinear system parameters of this structure (including electromechanical coupling, capacitance, etc.) can be found in the paper by Leadham and Erturk (2015).

3. Limitations and issues in resistive and resistive–inductive linear shunts

In passive piezoelectric shunt damping, the piezoelectric interface is shunted to simple passive electrical circuits where the mechanical energy converted into electrical energy through the direct piezoelectric effect is dissipated via Joule heating. The first applications from shunt damping literature are reported as a resistive circuit (Uchino and Ishii, 1988), inductive shunt circuit (Forward, 1979), resistive–inductive in series (Hagood and von Flotow, 1991), and resistive–inductive in parallel (Wu, 1996). Since the shunt circuit is tuned for a specific target frequency, the effective bandwidth of such a system is relatively small. An optimal resistor for maximum damping can be obtained in the resistive case (Uchino and Ishii, 1988); however, this is a relatively limited approach for suppressing the large-amplitude response of the weakly coupled nonlinear structure (Leadenham and Erturk, 2015). As can be seen in Figure 3, dissipation caused by the optimal resistive load results in small shortening of the large-amplitude branch of the nonlinear frequency response. Therefore, purely resistive shunting is unlikely to offer bifurcation suppression for this strongly nonlinear structure.

As for the resistive–inductive case, the inductor (L) must be tuned according to the target mechanical frequency and piezoelectric capacitance to have $L \sim 1/\omega^2 C_p$ (where ω is the frequency and C_p is the equivalent piezoelectric capacitance). In this experimental structure, since the equivalent capacitance is around

34 nF (Leadenham and Erturk, 2015), the required inductance for such low mechanical frequencies (14–15 Hz) is extremely high for passive implementation (around 3500 H) and complex synthetic inductance or synthetic impedance circuits (Fleming et al., 2000; Luo et al., 2009) become necessary. The SSDI circuit that is discussed next overcomes the large inductance requirement issue of linear inductive shunting while offering substantial damping performance.

4. Nonlinear synchronized switching circuits for vibration attenuation and energy harvesting

SSD techniques (Guyomar et al., 2009; Lefeuvre et al., 2006; Richard et al., 1999, 2000) were developed in order to address the limitations in passive shunt damping methodologies as well as the issues associated with active control systems (Ahmadian and Deguilio, 2001; Lesieutre, 1998). The SSD techniques are semi-passive or semi-active methods that introduce the nonlinear treatment of the electrical output of piezoelectric elements and induce an increase in mechanical to electrical energy conversion in systems with weak electromechanical coupling. In the semi-passive approaches considered in this work, the piezoelectric material is kept in the open-circuit condition except for a small period of time, where voltage is either canceled due to a switch to a small resistance (SSDS) or inverted due to brief switch to an inductor (SSDI). In both cases, switching is performed synchronously with mechanical displacement; therefore, the voltage output of the piezoelectric material is in phase with the structural velocity (resulting in enhanced attenuation along each cycle of oscillation). In the SSDI case, the electrical resonance frequency is much larger than that of the mechanical resonance frequency of interest. Consequently, the inductance values in semi-passive nonlinear SSDI are substantially smaller (typically by orders of magnitude) than the inductance requirement of fully passive linear inductive shunt circuits.

The schematic representations of the nonlinear SSDS and SSDI techniques can be seen in Figure 4(a) and (b), where the piezoelectric voltage is V_p , the inductance in the latter is L , and the internal (parasitic) wire resistance in both techniques is R . The energy-harvesting implementation of the SSDI circuit is the SSHI technique as originally proposed by Guyomar et al. (2005). In the absence of an AC–DC conversion circuit (introduced later in section “Nonlinear vibration attenuation: numerical and experimental results”), for an electrical load of R_H , the SSHI circuit has the form of Figure 4(c) (for AC input–AC output).

In nonlinear synchronized switching shunts, the piezoelectric element is intermittently switched from open-circuit to a specific electrical boundary condition

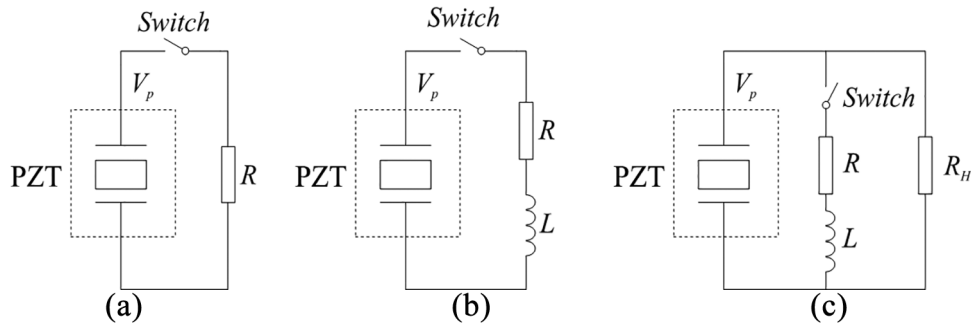


Figure 4. Nonlinear switching circuits employed in this work for shunt damping of the nonlinear structure: (a) synchronized switch damping on short circuit (SSDS) and (b) synchronized switch damping on inductor (SSDI) circuit; and (c) energy harvesting implementation of the synchronized switch on inductor circuit (SSHI) in the absence of AC–DC conversion. Note that for the ideal case of zero wire resistance $R = 0$.

synchronously with the structural motion. The control principles of SSDS and SSDI techniques are based on detecting the maximum as well as the minimum voltage values (switching points). More specifically, in the SSDI circuit, the switch is briefly closed when a displacement (or voltage) extrema is detected (details can be found in studies by Fleming et al. (2000), Guyomar et al. (2005), Luo et al. (2009), and Richard et al., 1999, 2000). Therefore, the internal capacitance of the piezoelectric element (C_p) and the inductance (L) constitute a resonant circuit. The voltage of the piezoelectric element is inverted after half period of the resonant circuit (Δt_i) when the switch is open again (Lallart et al., 2008). The inversion time is proportional to the inductance as

$$\Delta t_i = \left(\frac{T}{2}\right) = \pi\sqrt{LC_p} \quad (4)$$

where T is the period of oscillation of the electrical circuit. The inductance L is chosen to give an inversion time that is 10–50 times smaller than the period of mechanical oscillation (Badel et al., 2007). As a result, the SSDI technique requires inductance values two to three orders of magnitude lower than the inductances required in passive resistive–inductive linear circuits, which alleviates the issue discussed in the previous section. This is particularly important for low-frequency vibration of flexible structures as in this work.

Self-powered implementation of switching is essential for the effective implementation of the SSDS and SSDI circuits. A self-powered nonlinear interface with an electronic breaker proposed by Richard et al. (2007) is displayed in Figure 5. This is one of the most popular self-powered analog approaches presented in the literature to autonomously detect the voltage extrema and is also implemented in our current work. Passive and semiconductor electronic components are used to

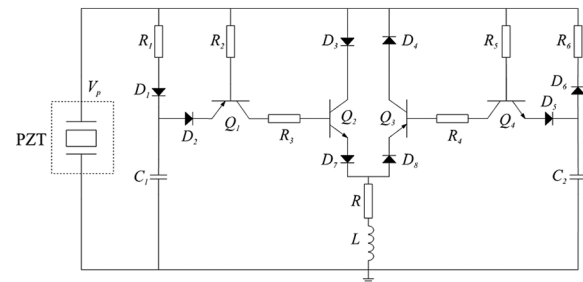


Figure 5. Self-powered full-wave electronic breaker circuit implemented in SSDI technique (based on Richard et al. (2007)).

detect the switching points by comparing the voltage output of the piezoelectric material with its delayed version. Three basic functions are addressed in Figure 5: an envelope detector (R_1, C_1 , and D_1), a comparator (R_2, D_2 , and Q_1), and a switch (D_3, R_3 , and Q_2), where R is a resistor, C is a capacitor, D is a diode, and Q is a transistor. The voltage of the piezoelectric element is compared (using the transistor Q_1 of the comparator R_2, D_2, Q_1) to its delayed counterpart obtained using the envelope detector (R_1, C_1, D_1). The transistor Q_1 is blocked while the delayed voltage (voltage at C_1) is smaller than the voltage of the piezoelectric element. The transistor Q_1 is conducted when the delayed voltage is larger than the piezoelectric voltage and the threshold of Q_1 . Since the transistor Q_1 is conducted, the transistor Q_2 is triggered, and the switching process (on short circuit with $R \rightarrow 0$ or on an inductor L) is started. The minimum voltage detection and switching is similar to the maximum one. In such case, another envelope detector (R_6, C_2 , and D_6), comparator (R_5, D_5 , and Q_4) and switch (D_4, R_4 , and Q_3) are employed. Self-powered SSDS and SSDI (and later the SSHI) circuits combined with the nonlinear structure shown in Figure 1 will be explored in the next sections both numerically and experimentally.

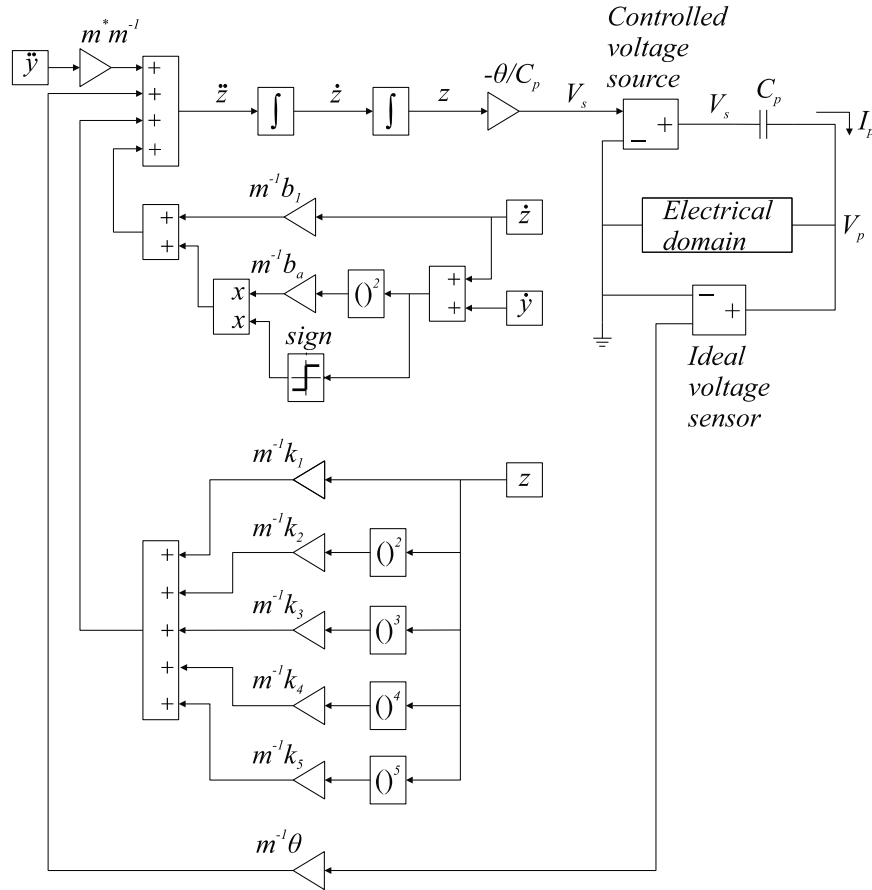


Figure 6. MATLAB Simulink block diagram constructed for simulating the dynamics of the nonlinear mechanical structure shunted to a nonlinear switching circuit in the electrical domain.

5. Nonlinear vibration attenuation: numerical and experimental results

5.1. Simulink model and numerical results

Simulations of the nonlinear electromechanically coupled structure with nonlinear switching circuits are carried out in MATLAB Simulink. The Simulink model is shown in Figure 6 for the general setting in this work. For simulation purposes, the governing equations of the electromechanical system, equations (1) and (2), are rearranged to give the following equations

$$\ddot{z} = (-m^{-1}b)\dot{z} + (-m^{-1}b_a)(\dot{y} + \dot{z})^2 \text{sgn}(\dot{y} + \dot{z}) + (-m^{-1}k_1)z + (-m^{-1}k_2)z^2 + (-m^{-1}k_3)z^3 + (-m^{-1}k_4)z^4 + (-m^{-1}k_5)z^5 + (m^{-1}\theta)V_p + (-m^{-1}m^*)\ddot{y}$$

$$V_p = -\frac{Q_p}{C_p} - \frac{\theta}{C_p}z$$

In Figure 6, the terms inside a parenthesis in equation (5) stand for a gain block (triangular blocks). The

excitation is due to the base motion prescribed in Figure 1(b). Equation (6) can be rewritten as

$$V_p = -\frac{Q_p}{C_p} + V_s$$

where

$$V_s = -\frac{\theta}{C_p}z$$

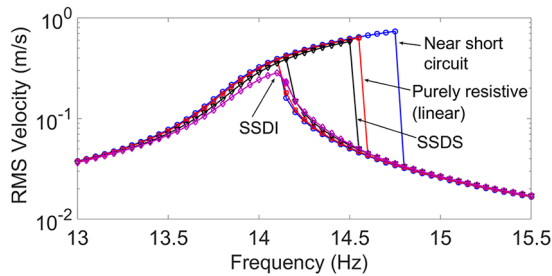
Equation (7) shows that the voltage output of the piezoelectric element (V_p) is equal to the voltage drop across a controlled voltage source (V_s) in series with the capacitor C_p . Therefore, the piezoelectric element is modeled as a controlled voltage source and a capacitor in series, as shown in Figure 6 and is connected to the block electrical domain. The electrical domain can account for different piezoelectric circuits (SSDS, SSDI, etc.). The function of the block “electrical domain” is to provide a relationship between V_p and Q_p for Simulink. This relationship along with equations (5) and (6) allows Simulink to calculate the three unknowns: z , V_p , and Q_p . It should be noted that the relation between V_p and Q_p is obtained in Simulink at

Table 1. Parameters of the nonlinear electromechanical coupled system.

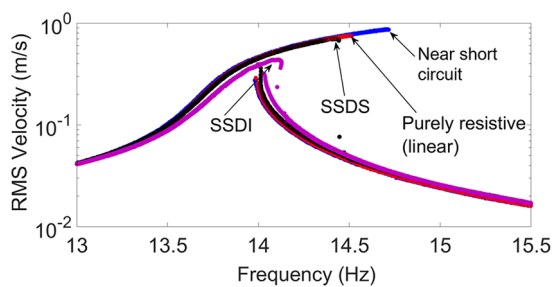
$m(\text{g})$	$b(\text{N s m}^{-1})$	$b_o(\text{N s}^2 \text{ m}^{-2})$	$\theta(\text{N V}^{-1})$	$C_p(\text{nF})$
31.9	5.5×10^{-3}	1.2×10^{-2}	1.7×10^{-4}	34.27
$k_1(\text{N m}^{-1})$	$k_2(\text{N m}^{-2})$	$k_3(\text{N m}^{-3})$	$k_4(\text{N m}^{-4})$	$k_5(\text{N m}^{-5})$
244.1	2860	363×10^3	10.3×10^6	210×10^6

Table 2. Parameters of the electrical components in the simulations and experiments.

Component	Value	Component	Value
R_1 and R_6	10 M Ω	R_2 to R_5	1 k Ω
C_1 and C_2	680 pF	C_r	330 nF
R	340 Ω	L	5 H
Q_2 and Q_4	MPSA92	Q_1 and Q_3	MPSA42
D_1 to D_{12}	FDH444	R_H	From 30 k Ω to 3 M Ω

**Figure 7.** Simulations of nonlinear frequency response curves (up- and down-sweep) showing near short-circuit behavior as the baseline, along with purely resistive, SSDS, and SSDI shunt circuits for damping of large-amplitude vibrations.

The SSDI case entirely eliminates the bifurcation. Base acceleration: 0.04g RMS.

**Figure 8.** Experimental nonlinear frequency response curves (up- and down-sweep) showing near short-circuit behavior as the baseline, along with purely resistive, SSDS, and SSDI shunt circuits for damping of large-amplitude vibrations (ideally for suppressing the bifurcations). Base acceleration: 0.04g RMS.

each time-step without any information coming from the user. This is advantageous when simulating complex electrical circuits such as SSDI (and its extension SSHI (Guyomar et al., 2005) in energy harvesting), since an equation that relates V_p and Q_p may not be

easy to express. However, if an electrical equation relating V_p and Q_p can be analytically obtained, it is convenient to use that relationship with equations (5) and (6) in state-space form. Simulations in the state-space form are faster than the proposed Simulink block diagram of Figure 6. It is worth mentioning that additional degrees of freedom can easily be incorporated in the Simulink model for a flexible structure with more than 1 degree-of-freedom (Cao et al., 2015).

Using the mechanical, electromechanical, and dielectric parameters of the nonlinear structure given in Table 1 (Leadenham and Erturk, 2015) along with nonlinear circuit parameters (Table 2), simulations are performed for a root-mean-square (RMS) base acceleration level of 0.04g. As shown in Figure 7 and as expected from Figure 3, the amount of large-amplitude branch shortening due to purely resistive shunting (Uchino and Ishii, 1988) even for the optimal resistor is relatively small, rendering resistive shunting method insufficient for eliminating the large-amplitude branch and suppressing the saddle-node bifurcations. The SSDS circuit results in significant improvement as compared to linear resistive shunting. Note that, as an alternative to using linear resistive shunting, if one aims to use linear inductive (Forward, 1979) or linear resistive-inductive (Hagood and von Flotow, 1991) shunting, the inductance requirement exceeds 3000 H which would mean a huge coil. On the other hand, the SSDI circuit case enables complete bifurcation suppression for an inductance value of only 5 H for this very-low-frequency nonlinear vibration damping problem. Note that the nonlinear treatment of voltage output from the piezoelectric material in both SSDS and SSDI changes the phase between piezoelectric voltage output and structural velocity, creating a mechanical force due to the converse coupling in the mechanical equation of motion (equation (1)). However, as compared to SSDS case, SSDI additionally exploits piezoelectric voltage

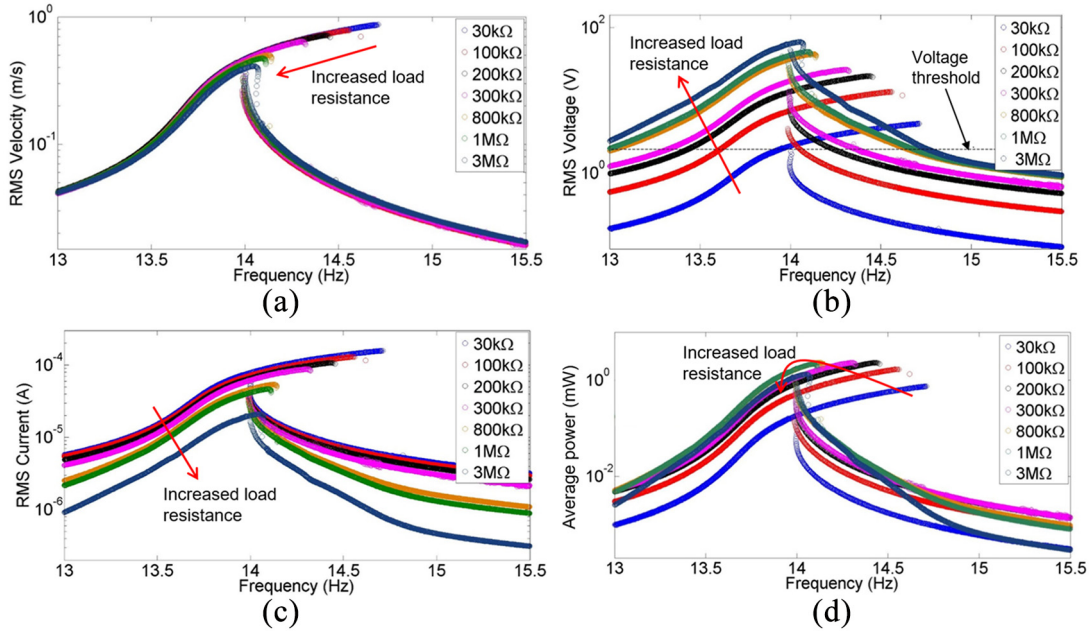


Figure 9. Experimental nonlinear frequency response curves (up- and down-sweep) showing the (a) RMS velocity, (b) RMS voltage, (c) RMS current, and (d) average electrical power for a set of electrical loads (AC input–AC output) with the SSHI circuit. Base acceleration: 0.04g RMS.

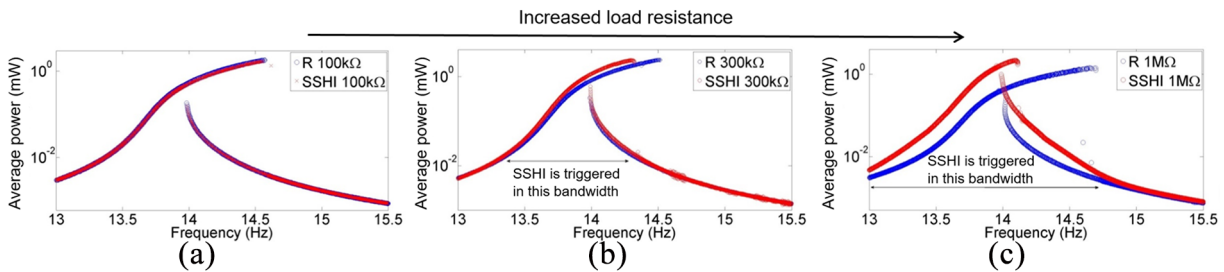


Figure 10. Comparison of linear resistive and SSHI energy harvesting circuits (AC input–AC output) for different load resistance values revealing that the power boost in SSHI is associated with substantially reduced bandwidth of the large-amplitude branch with increased load resistance (since SSHI converges to SSDI with increased harvester load). Base acceleration: 0.04g RMS (resistive load case is shown in blue, SSHI case is shown in red).

amplitude amplification, yielding enhanced vibration attenuation. In the next section, experiments are conducted to test this scenario for these system parameters.

5.2. Experimental results

For the same base acceleration level as in the numerical case study of Figure 7, experimental results are presented in Figure 8 using the setup that was shown in Figure 2(a). The baseline case near the short-circuit condition expectedly shows the largest (and undesired) frequency bandwidth for the large-amplitude branch. The optimal electrical load for the linear resistive load case (extracted from Figure 3) results in a small shortening of the large-amplitude branch, and as noted previously, the linear resistive–inductive loading case is impractical in this configuration due to the

aforementioned extremely large inductance requirement at such low frequencies. It is observed that the SSDS circuit offers larger damping and greater shortening of the large-amplitude branch than the purely resistive loading case, in agreement with the numerical simulations in Figure 7. However, the largest reduction in the large-amplitude branch is due to the SSDI circuit (Figures 4(b) and 5). While the bifurcations are not fully suppressed in the experimental case, the overall agreement between the numerical and experimental results in Figures 7 and 8 is very good.

6. Nonlinear wideband energy harvesting implications

It is well-known that the SSHI circuit substantially enhances the resonant electrical power output in

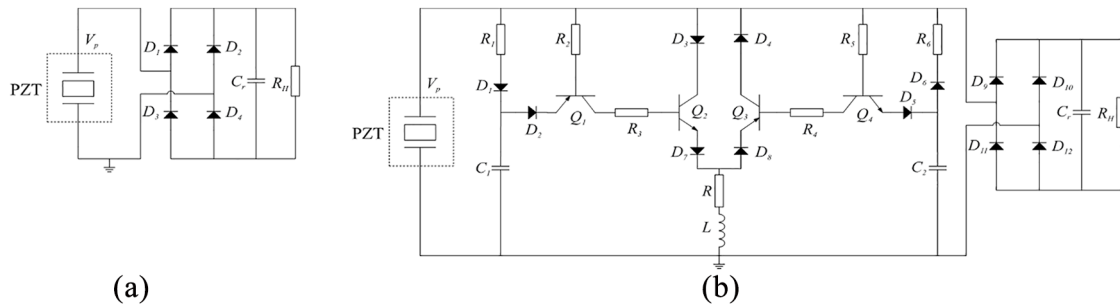


Figure 11. AC–DC conversion circuits using a full-wave rectifier for (a) purely resistive load and (b) SSHI circuit with a resistive load.

piezoelectric energy harvesting for weakly coupled, structurally linear configurations (Guyomar et al., 2005). However, it is rather unknown how this effective switching circuit interacts with the large-amplitude branch of intentionally designed geometrically nonlinear energy harvesters. In the existing literature, nonlinear wideband energy harvesting efforts that exploited designed geometric/structural nonlinearities typically ignore circuit nonlinearities (examples can be found in the comprehensive review article by Daqaq et al. (2014)); and likewise, nonlinear electrical circuit studies (Guyomar et al., 2005), such as the SSHI case, have typically assumed linear mechanical behavior. This section is an attempt to bridge the nonlinear SSHI circuit with a strongly nonlinear energy-harvester structure (the same structure considered so far –Figures 1 and 2). For all experimental cases below, the base acceleration level is 0.04g RMS (as in the shunt damping studies given in the previous sections).

Figure 9 shows the electromechanical frequency response curves (velocity, voltage, current, and power) of the nonlinear energy-harvester structure with SSHI circuit. According to Figure 9(a), the large-amplitude branch monotonically shortens with increased load resistance (R_H). In fact, a careful investigation of Figure 4(b) and (c) shows that the extreme of $R_H \rightarrow \infty$ in SSHI setting corresponds to SSDI circuit, yielding the maximum vibration attenuation scenario in this work. From another point of view, the load resistance provides a parameter to tailor the large-amplitude branch shortening in SSDI. In Figure 9(a), ultimately for $R_H = 3 \text{ M}\Omega$, the large-amplitude energy branch is almost suppressed entirely (reduced to a bandwidth of 0.07 Hz). The trends in the voltage (Figure 9(b)) and the current (Figure 9(c)), which are the opposite of each other with changing load resistance, are expected (even from totally linear configurations (Erturk and Inman, 2011)), other than multi-valued response due to the nonlinearity and the resulting bifurcations. Note that the self-powered SSHI circuit is triggered only above a certain voltage level as marked in Figure 9(b) (2.1 V RMS voltage, or a voltage amplitude of 3 V). Once the

SSHI is triggered, the voltage output is boosted; otherwise (for voltages below the threshold), the results are the same as the linear resistive electrical loading that was studied in detail by Leadenham and Erturk (2015). Remarkably, the maximum power level in Figure 9(d) can be obtained over a range of frequencies as long as the load resistance is altered (in the 200–800 k Ω range), forming a plateau of the maximum power output. Most importantly, the SSHI circuit results in significant reduction of the large-amplitude bandwidth that was owed to the designed structural nonlinearity. The next logical question is whether the use of SSHI is useful or entirely drastic in this mechanically nonlinear wideband energy harvester.

Figure 10 shows the comparison of linear resistive and nonlinear SSHI circuits for three different load resistance values that cover a critical range (optimal load neighborhood for the maximum power in both configurations). In the first case ($R_H = 100 \text{ k}\Omega$; Figure 10(a)), the piezoelectric voltage output is not high enough to overcome the threshold of the nonlinear circuit. When the threshold is not exceeded, the switch of the SSHI case is kept in the open circuit (OC) condition, and therefore, the harvester is continuously connected to the resistance R_H , yielding results identical to the linear resistive load case. After increasing R_H to 300 k Ω (Figure 10(b)), the piezoelectric voltage increases and the nonlinear circuit is triggered over the frequency range of 13.4–14.35 Hz. In this bandwidth, the SSHI circuit provides more power output than the resistive case on the large-amplitude branch. However, beyond 14.35 Hz, there is no large-amplitude branch for the SSHI circuit, whereas that of the resistive circuit extends to 14.51 Hz (Figure 10(b)). In other words, the shunt damping effect of the SSHI circuit reduces the bandwidth of the harvester as compared to the resistive circuit, as a main trade-off associated with increased power. This trade-off is even more visible and significant in Figure 10(c) for the case of 1 M Ω load resistance. There is wider a range of frequencies for which the SSHI circuit is triggered and outperforms the resistive circuit case; however, the wideband large-amplitude

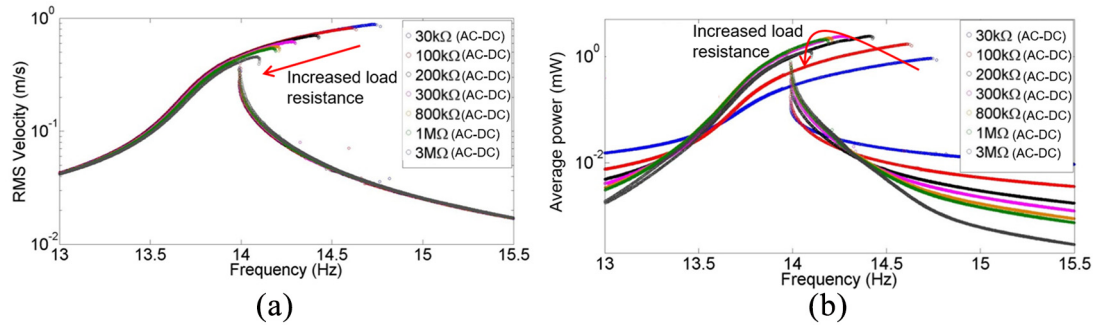


Figure 12. Experimental nonlinear frequency response curves (up- and down-sweep) showing the (a) RMS velocity and (b) average electrical power for a set of electrical loads (AC input–DC output) with the SSHI circuit. Base acceleration: 0.04g RMS.

characteristics of the harvester emerging from the structural (i.e. mechanical) nonlinearity is drastically reduced. This is an inevitable result of the strong shunt damping effect of the switch on inductor circuit (as the load resistance is increased, the SSHI circuit converges to the SSDI circuit that was discussed in the previous sections). Nevertheless, moderate load resistance values that provide some boost in the voltage output without entirely eliminating the wideband branch of the nonlinear structure can be preferred. It should also be mentioned that there is a clear advantage of the SSHI circuit in the small-amplitude response branch associated with down-sweep in Figure 10(c) as long as the self-powered switching circuit is triggered.

Finally, it is worth exploring a more realistic energy-harvesting scheme by including a full-wave rectifier for standard AC–DC conversion (Shu et al., 2007; Shu and Lien, 2006). A typical AC–DC conversion circuit is shown in Figure 11(a), in which the diode bridge is followed by a filter (smoothing) capacitor to obtain a stable DC voltage output. In the presence of a self-powered SSHI circuit, the AC–DC conversion scheme takes the form of Figure 11(b) (in view of Figure 5). The up- and down-sweep experimental results are shown in Figure 12. The overall qualitative behavior is the same as that in the absence of the rectifier; therefore, only the vibration and electrical power frequency response curves are shown. It is reasonable to expect that the SSHI circuit may provide some enhancement in the harvested power locally at certain frequencies (as in Figure 10). However, the wideband behavior of the harvester structure is again significantly reduced for large electrical load values due to the significant shunt damping performance that almost suppressed the large-amplitude branch for the extreme case of SSDI.

7. Conclusion

Piezoelectric shunt damping methods (passive and semi-passive techniques) have thus far been implemented for linear vibration of flexible structures with single-valued linear frequency response functions. However,

such flexible structures can easily undergo undesired bifurcations and exhibit nonlinear large-amplitude vibrations that coexist with small-amplitude vibrations in their frequency response. In this work, a strongly nonlinear and weakly coupled flexible structure shunted to two types of nonlinear synchronized switch damping circuits was explored for suppression of nonlinear bifurcations associated with the geometric nonlinearity. SSDS circuit and SSDI circuit techniques were employed and compared with the baseline (near short circuit) and optimal resistive loading frequency response curves of the flexible nonlinear structure. Through numerical simulations and carefully conducted experiments, it was shown that the SSDI circuit can substantially reduce the large-amplitude branch, offering the possibility of entirely suppressing bifurcations of the nonlinear system. It was also shown that simple resistive shunting cannot achieve sufficient shortening of the large-amplitude branch, and resistive–inductive shunting is impractical especially for low-frequency implementation due to drastically large inductance requirements (on the order of 3000 H in this work).

The energy harvesting circuit counterpart of SSDI, namely the SSHI circuit, was also explored for the same strongly mechanically nonlinear and wideband structure. It is known that SSHI circuit increases the power output for weakly coupled, structurally (i.e. mechanically) linear energy harvesters. In this work, we studied the performance of an SSHI circuit with this strongly nonlinear harvester structure that is employed as a wideband energy harvester. It was observed that the SSHI circuit can boost the voltage output of the large-amplitude branch for certain frequencies as compared to linear resistive loading. However, as the electrical load resistance is increased, the SSHI circuit converges to the SSDI circuit, and the wideband large-amplitude branch of the harvester substantially shrinks due to the aforementioned strong shunt damping characteristics as a trade-off. Nevertheless, for moderate electrical load resistance values, the electrical power can be boosted without entirely eliminating the

wideband behavior emerging from the mechanical non-linearity. There is also a clear advantage of the SSHI circuit in the small-amplitude response branch provided that the self-powered switching circuit is triggered.

Declaration of conflicting interests

The author(s) declared no potential conflicts of interest with respect to the research, authorship, and/or publication of this article.

Funding

The author(s) disclosed receipt of the following financial support for the research, authorship, and/or publication of this article: The authors gratefully acknowledge support from the São Paulo Research Foundation (FAPESP) (Grant No.: 2015/11325-3), CAPES of Brazil (Grant No.: 99999.003755/2015-00), and the U.S. National Science Foundation (Grant No.: CMMI-1254262).

ORCID iDs

Carlos De Marqui, Jr.  <https://orcid.org/0000-0003-4058-1885>

Alper Erturk  <https://orcid.org/0000-0003-0110-5376>

References

- Ahmadian M and Degulio AP (2001) Recent advances in the use of piezoceramics for vibration suppression. *The Shock and Vibration Digest* 33: 15–22.
- Badel A, Lagache M, Guyomar D, et al. (2007) Finite element and simple lumped modeling for flexural nonlinear semi-passive damping. *Journal of Intelligent Material Systems and Structures* 18: 727–742.
- Bandstra J (1983) Comparison of equivalent viscous damping and nonlinear damping in discrete and continuous vibrating systems. *Journal of Vibration, Acoustics, Stress, and Reliability in Design* 105: 382–392.
- Caio D, Leadenham S and Erturk A (2015) Internal resonance for nonlinear vibration energy harvesting. *The European Physical Journal—Special Topics* 224: 2867–2880.
- Clark WW (2000) Vibration control with state-switched piezoelectric materials. *Journal of Intelligent Material Systems and Structures* 11: 263–271.
- Corr LR and Clark WW (2002) Comparison of low-frequency piezoelectric switching shunt techniques for structural damping. *Smart Materials and Structures* 11: 370–376.
- Cunefare KA, De Rosa S, Sadegh N, et al. (2000) State-switched absorber for semi-active structural control. *Journal of Intelligent Material Systems and Structures* 11: 300–310.
- Daqaq MF, Masana R, Erturk A, et al. (2014) On the role of nonlinearities in vibratory energy harvesting: a critical review and discussion. *Applied Mechanics Reviews* 66: 040801.
- Erturk A and Inman DJ (2011) *Piezoelectric Energy Harvesting*. Chichester: Wiley.
- Fleming A, Behrens S and Moheimani S (2000) Synthetic impedance for implementation of piezoelectric shunt-damping circuits. *Electronics Letters* 36: 1525–1526.
- Forward RL (1979) Electronic damping of vibrations in optical structures. *Applied Optics* 18: 690–697.
- Guckenheimer J and Holmes P (2013) *Nonlinear Oscillations, Dynamical Systems, and Bifurcations of Vector Fields*. Berlin: Springer Science + Business Media.
- Guyomar D, Badel A, Lefeuvre E, et al. (2005) Toward energy harvesting using active materials and conversion improvement by nonlinear processing. *IEEE Transactions on Ultrasonics, Ferroelectrics, and Frequency Control* 52: 584–595.
- Guyomar D, Mohammadi S and Richard C (2009) Effect of boundary (support) conditions on piezoelectric damping in the case of SSDI vibration control technique. *Mechanical Systems and Signal Processing* 23: 501–513.
- Hagood NW and Crawley EF (1991) Experimental investigation into passive damping enhancement for space structures. *Journal of Guidance, Control, and Dynamics* 14: 1100–1109.
- Hagood NW and von Flotow A (1991) Damping of structural vibrations with piezoelectric materials and passive electrical networks. *Journal of Sound and Vibration* 146: 243–268.
- Jones DI (2001) *Handbook of Viscoelastic Vibration Damping*. Hoboken, NJ: John Wiley & Sons.
- Kovacic I and Brennan MJ (2011) *The Duffing Equation: Nonlinear Oscillators and Their Behaviour*. Hoboken, NJ: John Wiley & Sons.
- Lallart M, Lefeuvre E, Richard C, et al. (2008) Self-powered circuit for broadband, multimodal piezoelectric vibration control. *Sensors and Actuators, A: Physical* 143: 377–382.
- Leadenham S and Erturk A (2015) Nonlinear M-shaped broadband piezoelectric energy harvester for very low base accelerations: primary and secondary resonances. *Smart Materials and Structures* 24: 055021.
- Lefeuvre E, Badel A, Petit L, et al. (2006) Semi-passive piezoelectric structural damping by synchronized switching on voltage sources. *Journal of Intelligent Material Systems and Structures* 17: 653–660.
- Lesieutre GA (1998) Vibration damping and control using shunted piezoelectric materials. *The Shock and Vibration Digest* 30: 187–195.
- Lossouarn B, Deü J-F and Kerschen G (2017) Passive realization of a nonlinear piezoelectric tuned vibration absorber with a saturable inductor. Available at: <https://congressline.hu/enoc2017/abstracts/295.pdf>
- Luo C, Whitehead M and Hofmann H (2009) Design and testing of a power electronic synthetic inductor. *International Journal of Electronics* 96: 1249–1264.
- Nashif AD, Jones DI and Henderson JP (1985) *Vibration Damping*. Hoboken, NJ: John Wiley & Sons.
- Nayfeh AH and Balachandran B (2008) *Applied Nonlinear Dynamics: Analytical, Computational and Experimental Methods*. Hoboken, NJ: John Wiley & Sons.
- Richard C, Guyomar D and Lefeuvre E (2007) Self-powered electronic breaker with automatic switching by detecting maxima or minima of potential difference between its power electrodes (FR2005/003000, publication number:

- WO/2007/063194). Available at: <https://patentscope.wipo.int/search/en/detail.jsf?docId=WO2007063194>
- Richard C, Guyomar D, Audigier D, et al. (1999) Semi-passive damping using continuous switching of a piezoelectric device. In: *1999 symposium on smart structures and materials*, pp. 104–111. International society for optics and photonics. Available at: <https://www.spiedigitallibrary.org/conference-proceedings-of-spie/3672/0000/Semi-passive-damping-using-continuous-switching-of-a-piezoelectric-device/10.1117/12.349773.short?SSO=1>
- Richard C, Guyomar D, Audigier D, et al. (2000) Enhanced semi-passive damping using continuous switching of a piezoelectric device on an inductor. In: *SPIE's 7th annual international symposium on smart structures and materials*, pp. 288–299. International Society for Optics and Photonics. Available at: <https://www.spiedigitallibrary.org/conference-proceedings-of-spie/3989/0000/Enhanced-semi-passive-damping-using-continuous-switching-of-a-piezoelectric/10.1117/12.384569.short>
- Shu Y and Lien I (2006) Analysis of power output for piezoelectric energy harvesting systems. *Smart Materials and Structures* 15: 1499.
- Shu Y, Lien I and Wu W (2007) An improved analysis of the SSHI interface in piezoelectric energy harvesting. *Smart Materials and Structures* 16: 2253.
- Silva T, Tan D, De Marqui C, et al. (2016) Suppression of nonlinear bifurcations in flexible structures using nonlinear switching shunt damping circuits. In: *ASME 2016 international design engineering technical conferences and computers and information in engineering conference*, American Society of Mechanical Engineers (V008T010A063-V008T010A063). Available at: <http://proceedings.asmedigitalcollection.asme.org/proceeding.aspx?articleid=2592209>
- Soltani P and Kerschen G (2015) The nonlinear piezoelectric tuned vibration absorber. *Smart Materials and Structures* 24: 075015.
- Sugino C, Leadenham S, Ruzzene M, et al. (2017) An investigation of electroelastic bandgap formation in locally resonant piezoelectric metastructures. *Smart Materials and Structures* 26: 055029.
- Uchino K and Ishii T (1988) Mechanical damper using piezoelectric ceramics. *Journal of the Ceramic Society of Japan* 96: 863–867.
- Vakakis AF, Gendelman OV, Bergman LA, et al. (2008) *Nonlinear Targeted Energy Transfer in Mechanical and Structural Systems*. Berlin: Springer Science + Business Media.
- Wu S-y (1996) Piezoelectric shunts with a parallel RL circuit for structural damping and vibration control. In: *1996 symposium on smart structures and materials*, pp. 259–269. International Society for Optics and Photonics. Available at: <https://www.spiedigitallibrary.org/conference-proceedings-of-spie/2720/0000/Piezoelectric-shunts-with-a-parallel-R-L-circuit-for-structural/10.1117/12.239093.short>
- Wu S-y, Turner TL and Rizzi SA (2000) Piezoelectric shunt vibration damping of an F-15 panel under high-acoustic excitation. In: *SPIE's 7th annual international symposium on smart structures and materials*, pp. 276–287. International Society for Optics and Photonics. Available at: <https://www.spiedigitallibrary.org/conference-proceedings-of-spie/3989/0000/Piezoelectric-shunt-vibration-damping-of-an-F-15-panel-under/10.1117/12.384568.short>
- Zhou B, Thouverez F and Lenoir D (2014) Essentially nonlinear piezoelectric shunt circuits applied to mistuned bladed disks. *Journal of Sound and Vibration* 333: 2520–2542.